American Mineralogist, Volume 104, pages 1043–1050, 2019

Lepageite, $Mn_3^{2+}(Fe_7^{3+}Fe_4^{2+})O_3[Sb_5^{3+}As_8^{3+}O_{34}]$, a new arsenite-antimonite mineral from the Szklary pegmatite, Lower Silesia, Poland

Adam Pieczka[1,*], Mark A. Cooper[2], and Frank C. Hawthorne[2]

[1]AGH University of Science and Technology, Department of Mineralogy, Petrography and Geochemistry, 30-059 Kraków, Mickiewicza 30, Poland. Orcid 0000-0002-2841-7313

[2]Department of Geological Sciences, University of Manitoba, Winnipeg, Manitoba R3T 2N2,Canada

Abstract

Lepageite, a new arsenite-antimonite mineral, was discovered in a granitic pegmatite hosted by serpentinites of the Szklary massif, Lower Silesia, southwest Poland. Lepageite is a primary mineral formed during injection of an evolved LCT-type melt related to anatectic processes within the metasedimentary-metavolcanic complex of the nearby Góry Sowie Block, ~380 Ma, into serpentinite of the Szklary massif and its contamination by fluid-mobile serpentinite-hosted elements, among others As and Sb, transported in the form of $H_2AsO_3^-$ and $HSbO_2$ species at pH ≈ 9–11 and a low redox potential of –0.7 to –0.3 V.

Keywords: Lepageite, new mineral, arsenite, antimonite, chemical composition, crystal structure, crystallization conditions, Szklary, Poland

Introduction

The Szklary pegmatite is a small body of granitic LCT (Li–Cs–Ta) pegmatite hosted by serpentinites of the Szklary massif, Lower Silesia, Poland. It is considered to be part of the tectonically fragmented Sudetic ophiolite (Majerowicz and Pin 1986) and is about 420 Ma old (Oliver et al. 1993). In spite of its small dimensions, the pegmatite is notable due to (1) the presence of many rare and unknown minerals of various mineral groups, e.g., native metals and metalloids, Nb-Ta and Mn oxides, Mn phosphates with the apatite-group and graftonite-group minerals richest in Mn worldwide, and numerous As-Sb accessory phases in the absence of typical löllingite and arsenopyrite; (2) very high degrees of Mn-Fe fractionation; and (3) the absence of sulfides and the occasional presence of baryte as the only phase containing sulfur (Pieczka 2010; Pieczka et al. 2011, 2013, 2015, 2018; Szuszkiewicz et al. 2018).

The assemblage of As-Sb minerals in the pegmatite (Table 1) evolves from zero-valent native As and Sb and their melts, through various As^{3+} and Sb^{3+} phases to pyrochlore-supergroup minerals in which As and Sb may occur also as pentavalent cations, and finally to As^{5+} substituting for P^{5+} in some phosphates. Such a sequence indicates the crystallization of the assemblage at varying Eh-pH conditions. Thus, considering valence states of As and Sb and other coexisting cations, the assemblage provides an opportunity to evaluate its formation conditions. In the paper, we discuss these conditions based on the composition of a newly discovered arsenite-antimonite mineral lepageite, ideally $Mn_3^{2+}(Fe_7^{3+}Fe_4^{2+})O_3[Sb_5^{3+}As_8^{3+}O_{34}]$. Lepageite has been approved by the Commission on New Minerals, Nomenclature and Classification (CNMNC) of the International Mineralogical Association (IMA 2018-028). The name of the mineral is for Yvon Le Page (born October 7, 1943), a crystallographer who (1) developed the program MISSYM that has played a major role in the correct solution of complex mineral structures (including lepageite itself), and (2) solved the structures of many minerals and was involved in the description of several new minerals. The lepageite holotype (specimen Sz 96) is deposited in the collection of the Mineralogical Museum of University of Wrocław, catalog number MMWr IV7926. The postal address of the museum is as follows: University of Wrocław, Faculty of Earth Science and Environmental Management, Institute of Geological Sciences, Mineralogical Museum, Poland.

Occurrence

Lepageite was discovered in the Szklary LCT pegmatite (50°39.068′N, 16°49.932′E), ~6 km north of the Ząbkowice Śląskie town, ~60 km south of Wrocław, Lower Silesia, southwest Poland. The massif is part of the Central-Sudetic ophiolite that adjoins the Góry Sowie Block (GSB) on the east. It is enclosed as a mega-boudin in the mylonitized GSB gneisses of the Early Carboniferous Niemcza Shear Zone. The pegmatite, completely excavated by mineral collectors in 2002, formed a north-northeast to south-southwest (NNE-SSW) elongated lens or a boudin ~4 × 1 m in planar section, outcropped in the northern part of the massif. To the southwest, it has a primary intrusive contact with an altered aplitic gneiss up to 2 m thick, and both rocks are surrounded by tectonized serpentinite (Szuszkiewicz et al. 2018). A vermiculite-chlorite-talc zone is locally present along the contact with serpentinite. The pegmatite corresponds to the beryl–columbite–phosphate subtype of the *REL*-Li pegmatite class in the classification of Černý and Ercit (2005). The pegmatite [383 ± 2 Ma; CHIME dating on monazite-(Ce), Pieczka et al. 2015] is significantly older than the neighboring small late-syntectonic dioritic, syenitic, and granodioritic intrusions (~335–340 Ma) occurring in the Niemcza Shear Zone (Oliver et

* E-mail: pieczka@agh.edu.pl

0003-004X/19/0007–1043$05.00/DOI: https://doi.org/10.2138/am-2019-6903

TABLE 1. Minerals of the Szklary pegmatite containing As and Sb

Mineral	Formula
Metalloids	
Arsenic	As
Antimony	Sb
Stibarsen	AsSb
Paradocrasite	Sb_3As
Oxides and hydroxides	
Arsenolite/claudetite	As_2O_3
Senarmontite	Sb_2O_3
Stibiocolumbite	$SbNbO_4$
Stibiotantalite	$SbTaO_4$
Oxy-stibiomicrolite	$(Sb^{3+},Ca)_2Ta_2O_6O$
Calciobetafite (Sb-bearing)	$(Ca,Sb^{3+},\square)_2(Ti,Sb^{5+},Nb)_2(O,OH,\square)$
a U-Mn-As-Sb-Ta-Ti oxide	$[(Mn,Fe)_{<3}U_{>1}]_{\Sigma4}(As_2Sb_2)_{\Sigma4}[(Ta,Nb)_{>2}Ti_{<2}]_{\Sigma4}O_{20}$
Arsenites and antimonites	
Schafarzikite	$FeSb_2O_4$
Lepageite	$Mn_3^{2+}(Fe_7^{3+}Fe_4^{2+})O_3[Sb_5^{3+}As_8^{3+}O_{34}]$
Phosphates and arsenates	
Fluorapatite (Mn,As-bearing)	$(Ca,Mn)_5[(P,As)O_4]_3$
Pieczkaite (As-bearing)	$Mn_5[(P,As)O_4]_3$
Chernovite-(Y)	$YAsO_4$
Arsenogorceixite	$BaAl_3(AsO_4)(AsO_3OH)(OH)_6$
Silicates	
Dumortierite (As,Sb-bearing)	$Al_{7-(5x+4w+y)/3}(Ta,Nb)_xTi_w\square_{(2x+w+y)/3}BSi_{(3-y)}(Sb,As)_yO_{18-y}$ $y \le 1.5$ and $1-(5x+4w+y)/3 > x$ and $> y$
Holtite (As,Sb-bearing)	$Al_{7-(5x+4w+y)/3}(Ta,Nb)_xTi_w\square_{(2x+w+y)/3}BSi_{(3-y)}(Sb,As)_yO_{18-y}$ $y \le 1.5$ and $x > 1-(5x+4w+y)/3$ and $> w$ and $Ta > Nb$
Nioboholtite (As,Sb-bearing)	$Al_{7-(5x+4w+y)/3}(Ta,Nb)_xTi_w\square_{(2x+w+y)/3}BSi_{(3-y)}(Sb,As)_yO_{18-y}$ $y \le 1.5$ and $x > 1-(5x+4w+y)/3$ and $> w$ and $Ta < Nb$
Titanoholtite (As,Sb-bearing)	$Al_{7-(5x+4w+y)/3}(Ta,Nb)_xTi_w\square_{(2x+w+y)/3}BSi_{(3-y)}(Sb,As)_yO_{18-y}$ $y \le 1.5$ and $w > 1-(5x+4w+y)/3$ and $> x$
Szklaryite[a]	$Al_{7-(5x+4w+y)/3}(Ta,Nb)_xTi_w\square_{(2x+w+y)/3}BSi_{(3-y)}(Sb,As)_yO_{18-y}$ $y > 1.5$

[a] Classified within the dumortierite supergroup. Because the formulas of dumortierite-supergroup end-members do not reflect common presence of Sb+As in compositions of the supergroup minerals, the formulas of the minerals are presented in the form of the general supergroup formula (Pieczka et al. 2013) and additional relationships among the contents of Al, Nb+Ta, and Ti at the Al1 site and Sb+As at the Sb(As) site of the dumortierite structure, which must be fulfilled for each of the minerals.

al. 1993) and corresponds to the anatectic event in the adjacent GSB of 380–374 Ma (Van Breemen et al. 1988; Timmermann et al. 2000; Turniak et al. 2015).

The pegmatite consists mainly of plagioclase ($Ab_{99–82}An_{1–18}$), microcline perthite, quartz, and biotite, with minor Fe^{3+}-bearing schorl-dravite, spessartine, and muscovite. It is relatively poorly zoned with (1) a marginal graphic zone composed of albite + quartz ± minor-to-accessory biotite commonly altered to clinochlore + black tourmaline; (2) a coarser-grained intermediate graphic zone of microcline perthite + quartz + small quartz-tourmaline nests, with smaller amounts of albite and biotite, increased abundance of muscovite and spessartine, and accessory chrysoberyl present locally in muscovite aggregates; (3) a central zone of graphic microcline + quartz, in places developed as blocky feldspar with interstitial albite, rare muscovite, and no black tourmaline or biotite (Pieczka 2000; Pieczka et al. 2015). The aforementioned accessory minerals are present in zones 2 and 3. Most of them form crystals usually less than 1 mm in size, disseminated in quartz, microcline, albite, and muscovite.

Lepageite is an accessory mineral, occurring only as minute inclusions, reaching 30 μm in diameter (commonly ~5 μm), in (Mn,Be,Na,Cs)-bearing cordierite or close to it (Fig. 1). It is associated with other Fe-Mn-As-Sb oxides: schafarzikite and three or four unrecognized arsenite-antimonite phases of different (Fe+Mn)/(As+Sb) ratio, but rarer and even smaller than lepageite, harmotome, Ba-bearing microcline, baryte, and hematite. The (Cs,Mg)-bearing beryl, (Cs,Mg)-bearing muscovite, Cs-bearing phlogophite, and annite, paragonite, clinochlore, chamosite, vermiculite, and smectites are found as the replacement and breakdown products after cordierite.

PHYSICAL PROPERTIES

Lepageite forms small euhedral to subhedral, brownish-black, opaque crystals up to 20–30 μm in size, with a metallic luster (Fig. 1). Due to the tiny grain sizes and a very small amount of available material, streak, hardness, tenacity, and optical properties were not determined. The mineral does not show fluorescence, and no cleavage, fracture or parting were observed. Density was not measured for the same reasons; the density calculated on the basis of the empirical composition of the type lepageite and its unit-cell volume is 5.192 g/cm^3. Using the empirical formula and calculated density, the mean refractive index obtained from Gladstone-Dale relation (Mandarino 1979, 1981) is 2.21.

CHEMICAL COMPOSITION

Quantitative chemical analyses of lepageite were done at the Inter-Institute Analytical Complex for Minerals and Synthetic Substances at the University of Warsaw, Poland, using a Cameca SX 100 electron microprobe operating in wavelength-dispersive (WDS) mode with an accelerating voltage of 15 kV, a beam current of 10 nA, peak count-time of 20 s, background time of 10 s, and a beam diameter of 1–2 μm. Standards, analytical lines, diffracting crystals and mean detection limits (wt%) were as follows: diopside (Mg*K*α, TAP, 0.03), rhodonite (Mn*K*α, LIF, 0.10), hematite (Fe*K*α, LIF, 0.10), GaAs (As*L*α, TAP, 0.06), and InSb (Sb*L*α, PET, 0.08). Al, Si, P, Ti, Nb, and Ta were sought but were below the detection limits. The raw data were reduced with the PAP routine of Pouchou and Pichoir (1985). Analytical data on holotype material are given in Table 2. The empirical formula of lepageite, $(Fe^{3+}_{6.90}Fe^{2+}_{3.89}Mn^{2+}_{3.10}Mg_{0.16})_{\Sigma14.05}(As^{3+}_{8.32}Sb^{3+}_{4.68})_{\Sigma13.00}O_{37}$, was calculated on the basis of 37 O atoms per formula unit (apfu) and 13 As^{3+} + Sb^{3+} cations as indicated by the crystal structure of the mineral. Taking into account the results of the crystal-structure investigation (see below), the end-member formula of lepageite is $Mn_3^{2+}(Fe_7^{3+}Fe_4^{2+})O_3[Sb_5^{3+}As_8^{3+}O_{34}]$, corresponding to (in wt%): As_2O_3 30.68, Sb_2O_3 28.26, Fe_2O_3 21.67, FeO 11.14, and MnO 8.25.

POWDER DIFFRACTION DATA

Powder diffraction data could not be collected due to the scarcity of material. The X-ray powder diffraction pattern calculated from the refined crystal structure is reported in Supplemental[1] Table S1.

CRYSTAL STRUCTURE

A single grain, 7 × 20 × 30 μm and composed of two twinned crystals, was extracted; all other grains were <5 μm. The grain was an entirely entombed inclusion that needed to be physically broken out. Therefore, we coated the section with grease to avoid loss of the crystal during this process.

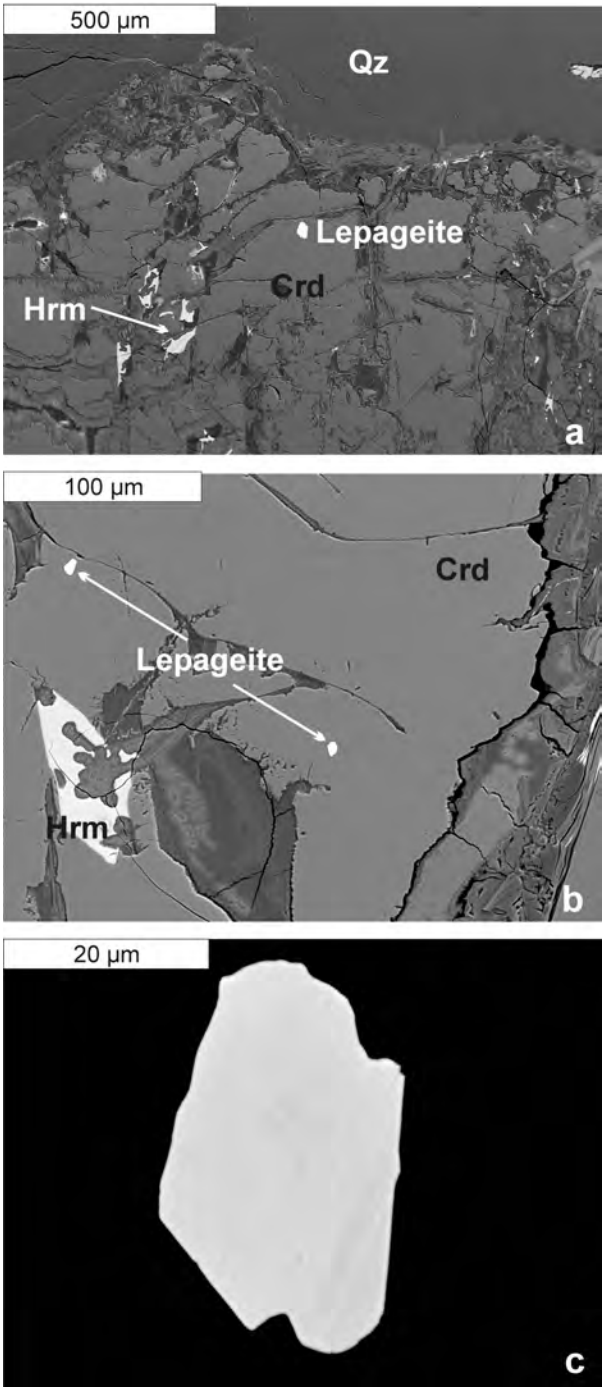

FIGURE 1. Characteristic appearance of lepageite in the Szklary pegmatite: (**a**) inclusion of the holotype crystal (before extraction) in (Mn,Be,Na,Cs)-bearing cordierite; (**b**) other representative inclusions of lepageite in cordierite; (**c**) holotype lepageite. Abbreviations: Crd = cordierite, Hrm = harmotome, Qz = quartz.

TABLE 2. Chemical composition of lepageite

Constituent	Mean (wt%)	Range (wt%)	S.D. (wt%)	Cation	apfu	S.D. (apfu)
As_2O_3	31.62	30.83–32.44	0.66	As^{3+}	8.32	0.17
Sb_2O_3	26.23	25.05–27.35	0.94	Sb^{3+}	4.68	0.17
Fe_2O_3	21.17	20.64–21.58	0.41	Fe^{3+}	6.90	0.13
FeO*	10.74	9.45–11.75	1.07	Fe^{2+}	3.89	0.39
MnO	8.44	7.88–9.27	0.59	Mn^{2+}	3.10	0.22
MgO	0.26	0.18–0.33	0.06	Mg^{2+}	0.16	0.04
Total	98.46					

Notes: *Total Fe as FeO (mean 29.79% FeO); S.D. = standard deviation.

Data collection and refinement

The extracted grain was attached to a MiTeGen polymer loop and mounted on a Bruker D8 three-circle diffractometer equipped with a rotating-anode generator (Mo$K\alpha$ X-radiation), multilayer optics and an APEX-II detector. A Ewald sphere of data was collected to 62 °2θ using 20 s per 0.2° frame with a crystal-detector distance of 5 cm. Evaluation of the diffraction pattern revealed that the crystal contained a significant non-merohedral twin-component (180° rotation about c*), and the intensity data were processed as an overlapping twin. Twin integration gave 94434 total reflections, with 32990 [component 1], 32911 [component 2], and 28533 [both components] (Supplemental[1] Material). The reflections were averaged and merged [R_{int} = 5.0%] to give 10478 reflections (single reflections from the primary domain, plus composites involving both domains) for structure (twin) refinement. The unit-cell dimensions were obtained by least-squares refinement of 4073 reflections with $I > 10\sigma I$. All diffraction maxima from the X-ray crystal can be indexed on the triclinic cell with the inclusion of the twin law [–0.998 –0.001 0.005/0.000 –1.000 –0.002/0.729 –0.025 0.998]. The *E* statistics are consistent with a center of symmetry, but attempts to solve the structure in the space group $P\bar{1}$ were unsuccessful. The atomic arrangement was solved in *P*1, and a center of symmetry was subsequently identified using the MISSYM program (Le Page 1987, 1988). An origin shift was applied and equivalent sites for the *P*1 model were combined to produce the $P\bar{1}$ structure model. Structure (twin) refinement from 10478 reflections (including 6350 composites) gave a final R_1 value of 3.6% (for 9912 observed reflections, $Fo > 4\sigma F$). The twin-volume fraction (i.e., twin contribution to composites) refined to 0.4756(7). Atom positions, equivalent isotropic-displacement parameters and selected interatomic distances there are in the attached CIF[1] file. Bond valences are given in Table 3.

Site assignment

The crystal structure of lepageite contains 28 cation sites and 37 anion sites. Lepageite is a simple oxide, in that the bond-valence sums at all O sites are in the range 1.85–2.14 v.u. (valence unit) (Table 3) and the O sites are occupied by simple O^{2-} ions. The cation sites can be subdivided into two groups: (1) those with a heavier scattering species, i.e., ≥ 33 *e*, with the cation displaced to one side of three or four O-sites; and (2) those possessing a lighter scattering species, i.e., ≤ 26 *e* that is centrally located with a [6]- to [8]-coordination. In the first group, the sites are occupied by As^{3+} and Sb^{3+} that show lone-pair-stereoactive behavior; in the second group, the sites are occupied by Fe^{3+}, Fe^{2+}, and Mn^{2+}.

The Sb(1)–Sb(4) sites are occupied by Sb^{3+} with two short equatorial bonds to O_{eq} (i.e., 1.93–2.03 Å) and two slightly longer axial bonds to O_{ax} (i.e., 2.12–2.35 Å), all lying to one side of the Sb^{3+} cation. The O_{ax}–Sb–O_{ax} angles vary from 141.9–145.4°, and the O_{eq}–Sb–O_{eq} angles vary from 95.3–105.7°. A similar coordination for Sb^{3+} occurs in stenhuggarite (Coda et al. 1977). Both the refined scattering and observed <[4]Sb-O> distances (i.e., 2.120–2.129 Å) are consistent with full occupancy of these sites

TABLE 3. Bond-valence table[a] for lepageite

	Sb(1)	Sb(2)	Sb(3)	Sb(4)	As(1)	As(2)	As(3)	As(4)	As(5)	As(6)	As(7)	As(8)[b]	As(9)	Mn(1)	Mn(2)	Mn(3)	Fe(1)	Fe(2)
O(1)		0.07		0.09	1.17	0.03	0.03	0.03										
O(2)		0.47			0.89													
O(3)				0.55	0.87													
O(4)			0.49	0.05		1.02				0.03								
O(5)	0.41		0.08			0.98											0.56	
O(6)				0.38		0.92												
O(7)							0.99									0.11		0.39,0.36
O(8)							0.92										0.46, 0.33	
O(9)							0.88											
O(10)			0.07				0.03	1.06							0.25			0.54
O(11)		0.05	0.45					1.06	0.03									
O(12)		0.43						0.84										
O(13)									1.00					0.36	0.28	0.27		
O(14)									1.00							0.18		
O(15)									0.99			0.04		0.11				
O(16)	0.07									1.04				0.41				
O(17)										1.01		0.05		0.05				
O(18)										0.99		0.05						
O(19)	0.12						0.06				1.10					0.04		
O(20)											1.09				0.40, 0.20	0.33		
O(21)	0.64										0.93				0.16			
O(22)												0.93						
O(23)												0.91						
O(24)												0.89						
O(25)													1.02	0.16		0.42		
O(26)			0.05										0.90				0.57	0.50
O(27)													0.87			0.12		0.45
O(28)	0.82																0.47	
O(29)	0.81		0.84											0.04	0.35			
O(30)		0.99, 0.06																
O(31)		0.86											0.08					
O(32)			0.88											0.32				
O(33)				0.97, 0.05														
O(34)				0.88														
O(35)													0.10				0.60	
O(36)															0.28	0.43		0.74
O(37)													0.03	0.42				
Σ	2.87	2.93	2.86	2.97	2.93	2.95	2.91	2.99	3.02	3.07	3.12	2.87	3.00	1.87	1.92	1.90	2.99	2.98

[a] Bond valences in v.u., bond-valence parameters from Gagné and Hawthorne (2015).
[b] As(8) site-occupancy ($As_{0.637}Sb_{0.363}$).

(Table extends on next page.)

by Sb^{3+}. There are longer Sb-O distances in each coordination polyhedron, resulting in the coordination numbers [6] and [7] ×3, respectively. These longer bonds contribute significantly to the sum of the incident bond-valences about the central cations, bringing the sums into accord with the valence-sum rule. The observed $<^{[6]}Sb^{3+}\text{-}O^{2-}>$ and $<^{[7]}Sb^{3+}\text{-}O^{2-}>$ distances are in accord with the mean distances observed in all inorganic oxide-oxysalt Sb^{3+} structures (Gagné and Hawthorne 2018): grand $<^{[6]}Sb^{3+}\text{-}O^{2-}>$ = 2.443 Å, range: 2.349–2.623 Å; $<^{[7]}Sb^{3+}\text{-}O^{2-}>$ = 2.486 Å, range: 2.445–2.517 Å.

The As(1)–As(9) sites are occupied dominantly by As^{3+} [with minor Sb^{3+} at As(8) and As(9)], with three short As-O bonds (i.e., 1.709–1.888 Å) to one side of the As^{3+} ion. This is a typical coordination for As^{3+} showing lone-pair-stereoactive behavior (e.g., Cooper and Hawthorne 1996, 2016). The refined scattering and $<^{[3]}As\text{-}O>$ distances (i.e., 1.783–1.806 Å) for the As(1)–As(7) sites are consistent with full occupancy by As^{3+}. Scattering in excess of 33 electrons was observed at the As(8) site, along with elongated As(8)-O bonds (i.e., $<^{[3]}As(8)\text{-}O>$ = 1.878 Å). Site-occupancy refinement with coupled As and Sb scattering factors gave $As_{0.637}Sb_{0.363}$ for the As(8) site. The excess scattering and greater bond lengths are in accord with the refined Sb content at As(8). The electron scattering around the As(9) site was modeled as two distinct sites [As(9a) and As(9b)] with a refined As(9a)–As(9b) distance of 0.640(19) Å. The refined site-occupancies for the As(9a) and As(9b) sites are 1.034(7) and 0.071(7), respectively; as the sum exceeds unity, the minor presence of an additional heavier scattering-species is indicated (i.e., Sb). The combined site-scattering of 36.5 *e* is consistent with an occupancy of $As_{0.81}$ and $Sb_{0.19}$ over the combined As(9a)/As(9b) sites. The As(9a) site has three short bonds to O ([<As(9a)-O> = 1.837 Å] and the As(9b) site has two shorter and two intermediate bonds to O (similar to the Sb sites). If the partitioning of As and Sb onto As(9a) and As(9b) is done with respect to ideal bond-valence constraint (i.e., 3 v.u.) at both sites, then the inferred occupancies of $^{As(9a)}(As_{0.80}Sb_{0.17})_{\Sigma 0.97}$ and $^{As(9b)}(As_{0.01}Sb_{0.02})_{\Sigma 0.03}$ result. The As and Sb contents from the chemical analysis is $(As_{8.32}Sb_{4.68})_{\Sigma 13}$ and from the site-occupancy refinement is $(As_{8.45}Sb_{4.55})_{\Sigma 13}$. For the sites occupied solely by As^{3+} [As(1)-As(7)], the mean bond-lengths for a coordination of [3] are very close and the incident bond-valence sums are close to 3 v.u. Gagné and Hawthorne (2018) list the grand $<^{[3]}As^{3+}\text{-}O^{2-}>$ distance as 1.789 Å with a range of 1.758 to 1.794 Å, and the values found here (1.759–1.789 Å) fall within this range. There are longer $As^{3+}\text{-}O^{2-}$ distances with suitable geometry that could correspond to weakly bonded ligands but they do not contribute significantly to the incident bond-valence sums.

There are three Mn sites occupied by Mn^{2+}. The Mn(1) and Mn(3) sites are coordinated by eight O^{2-} ions with <Mn-O> distances of 2.472 and 2.436 Å, respectively. These two Mn coordinations show significant overall bond-length dispersion,

TABLE 3.—*EXTENDED*

	Fe(3)	Fe(4)	Fe(5)	Fe(6)	Fe(7)	Fe(8)	Fe(9)	Fe(10)	Fe(11)	Σ
O(1)						0.56				1.99
O(2)				0.38					0.23	1.97
O(3)		0.38						0.22		2.05
O(4)								0.36		1.95
O(5)										2.03
O(6)	0.39					0.23				1.92
O(7)										1.85
O(8)					0.18					1.89
O(9)	0.39		0.40				0.27			1.94
O(10)										1.95
O(11)									0.37	1.96
O(12)			0.36			0.26				1.89
O(13)										1.91
O(14)			0.56				0.26			2.00
O(15)				0.54					0.38	2.06
O(16)					0.46					1.91
O(17)		0.54						0.37		2.02
O(18)	0.54						0.38			1.96
O(19)					0.68					1.88
O(20)										2.02
O(21)							0.29			2.02
O(22)		0.44, 0.21						0.30		1.88
O(23)	0.24		0.36			0.34				1.85
O(24)				0.42, 0.24					0.31	1.86
O(25)					0.43					
O(26)										
O(27)			0.56							
O(28)					0.29		0.33			1.91
O(29)										2.04
O(30)						0.46			0.43	1.94
O(31)			0.60	0.60						
O(32)								0.36	0.36	1.92
O(33)						0.48		0.43		1.93
O(34)	0.63	0.61								2.11
O(35)	0.71				0.49					1.90
O(36)							0.51			1.96
O(37)		0.76		0.69						1.90
Σ	2.90	2.94	2.84	2.87	2.53	2.33	2.04	2.04	2.08	

with individual Mn-O distances spanning 2.09–3.10 Å. The Mn(2) site is coordinated by seven O atoms with a <Mn(2)-O> distance of 2.300 Å. The refined site-occupancy at Mn(2) [1.065(7)] indicates that a minor amount of a heavier scattering species may be present (presumably Fe^{2+}). There are 11 Fe sites octahedrally coordinated by O atoms with <Fe-O> distances in the range 2.023–2.153 Å. The refined site-occupancies and mean bond-lengths are consistent with occupancy by a combination of Fe^{3+} and Fe^{2+}. The Fe(1)–Fe(6) sites have <Fe-O> distances from 2.023–2.052 Å and bond-valence sums (using the Fe^{3+}-O equation) from 2.84–2.99 v.u. (Table 3), indicating that these six Fe sites are predominantly occupied by Fe^{3+}. The Fe(9)–Fe(11) sites have <Fe-O> distances from 2.139–2.153 Å and bond-valence sums (using the Fe^{2+}-O bond-valence parameters) from 2.04–2.08 v.u. (Table 3), indicating that these three Fe sites are predominantly occupied by Fe^{2+}. The Fe(7) and Fe(8) sites have intermediate <Fe-O> distances of 2.106 and 2.124 Å and bond-valence sums (using the Fe^{3+}-O bond-valence parameters) of 2.53 and 2.33 v.u., respectively (Table 3), indicating that these two Fe sites are occupied by both Fe^{2+} and Fe^{3+}. All As and Sb ions in the structure occur in coordinations characteristic of the 3+ oxidation state. The three larger coordination polyhedra contain Mn that must be in the 2+ oxidation state as indicated by the <Mn-O> distances that are characteristic of Mn^{2+} and are in accord with both the electroneutrality of the structure and crystallization at low Eh conditions (see Genetic Implications).

Bond topology

The various cation polyhedra are named using the central site. Sb(1), Sb(2), Sb(3), Sb(4) and As(1), As(2), As(4), As(7) form a finite cluster of SbO_4 and AsO_3 groups (Fig. 2). $Sb(2)O_4$, $As(4)O_3$, $Sb(3)O_4$, $As(2)O_3$, $Sb(4)O_4$, and $As(1)O_3$ form a six-membered ring by sharing polyhedron corners with each other. The polyhedra are oriented with respect to the ring such that the stereoactive lone-pairs of electrons belonging to the Sb^{3+} ions are oriented inward toward the center of the ring, whereas the stereoactive lone-pairs of electrons belonging to the As^{3+} ions are oriented outward away from the center of the ring (Fig. 2). An $Sb(1)O_4$ group shares anions with an $Sb(3)O_4$ group and an $As(2)O_3$ group to form a three-membered ring that shares an edge with the six-membered ring, and the Sb(1)O4 group links to a (terminal) $As(7)O_3$ group. All AsO_3 groups in this cluster link only to SbO_4 groups, whereas $Sb(1)O_4$ links directly to $Sb(3)O_4$ in the three-membered ring (Fig. 2). All short As-O distances of the polyhedra in the cluster are close to their mean value of 0.98 v.u. However, the short Sb-O distances fall into two groups, with pairs of bonds in each cluster close to their mean values of 0.88 and 0.48 v.u., respectively. It is the longer Sb-O bonds (~0.48 v.u.) that link to the adjoining AsO_3 groups, allowing the bridging anions also to link to the Fe and Mn octahedra. The remaining AsO_3 groups involve As(3), As(5), As(6), As(8), and As(9), and are all isolated groups in that they do not link to each other or to the polyhedra of the cluster. Thus, there is no direct linkage of AsO_3 polyhedra in the structure of lepageite, and we may write the (Sb,As) component of the structure as $[Sb_4As_4O_{19}][AsO_3]_5$.

In the structure, Mn^{2+} is both [7]- and [8]-coordinated (Fig. 3a). The polyhedra share edges to form a cluster of six polyhedra that are centered at the origin of the structure. Three Fe^{2+} octahedra, Fe(5), Fe(8), and Fe(9), share edges to form a staggered trimer (Fig. 3b). The remaining Fe octahedra form an extended group of staggered chains of edge-sharing and corner-sharing octahedra linked together by sharing corners with single octahedra (Figs. 4a and 4b). These three elements form a densely packed framework with the Sb^{3+} and As^{3+} polyhedra (Fig. 5).

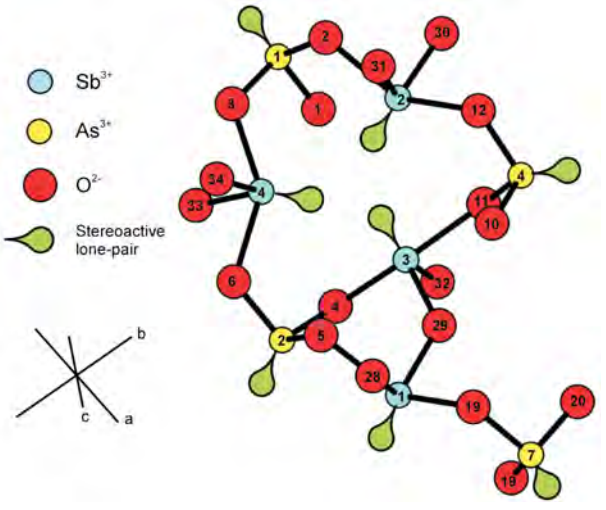

FIGURE 2. The $[Sb_4As_4O_{19}]$ cluster in the crystal structure of lepageite.

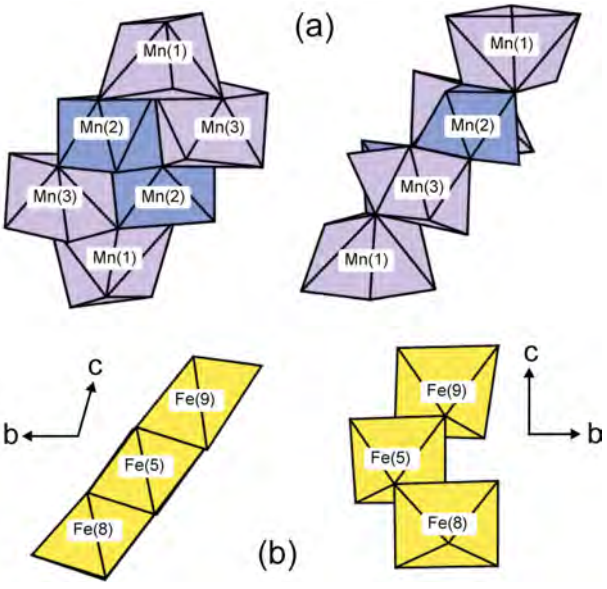

FIGURE 3. Components of the structure of lepageite: (**a**) the cluster of $Mn^{2+}O_7$ groups (blue polyhedra) and $Mn^{2+}O_8$ groups (lilac polyhedra); (**b**) the trimer of $Fe^{2+}O_6$ octahedra (yellow polyhedra).

Chemical formula

The O(1)–O(27) anions are the 27 O atoms involved in the nine AsO_3 groups. The anions O(30), O(31), O(33), and O(34) form short bonds with Sb^{3+} at Sb(2) and Sb(4), and collectively can be represented as two SbO_2 groups. The anions O(28), O(29), and O(32) form short bonds with Sb(1) and Sb(3) where O(29) is a bridging O atom, thus forming a Sb_2O_3 group. The remaining anions O(35), O(36), and O(37) form stronger bonds to the Mn and Fe sites. The Mn^{2+} is highly ordered at the three Mn sites, whereas there is some disorder in the Fe^{2+}-Fe^{3+} distribution. The divalent cations from the chemical analysis involve 3 elements (Fe^{2+}, Mn^{2+}, Mg^{2+}), and the overall 2+ and Fe^{3+} content is fixed by stoichiometry in relation to the constituent 37 O apfu. Thus, for $(As^{3+},Sb^{3+})_{13}(Fe^{3+},Fe^{2+},Mn^{2+},Mg)_{14}O_{37}$, the Fe^{3+} content must be 7 apfu, and the chemical data were so normalized. The formula $Mn^{2+}_3(Fe^{3+}_7Fe^{2+}_4)O_3[Sb^{3+}_4As^{3+}_9O_{34}]$ conveys these attributes. Lepageite is in class 04.JA. Arsenites, antimonites, bismuthites; without additional anions, without H_2O in the classification of Strunz (Strunz and Nickel 2001), and in the classification of Dana (Gaines et al. 1997), it belongs to class 45. Acid and normal antimonites and arsenites.

IMPLICATIONS

Arsenites and antimonites are rare in nature (<50 mineral species) and are generally related to base-metal and polymetallic ore deposits, usually as accessory phases associated with more common As and Sb minerals such as arsenopyrite, löllingite, tetrahedrite, etc. Of the ~20 arsenite ± antimonite minerals of Fe ± Mn, only karibibite and schneiderhöhnite have been discovered in pegmatites: karibibite, $Fe^{3+}_3(As^{3+}O_2)_4(As^{3+}_2O_5)(OH)$, first at Tuften, Norway (Larsen 2013), and karibibite + schneiderhöhnite, $Fe^{2+}Fe^{3+}_3As^{3+}_5O_{13}$, in pegmatites of the Kalba Range, Kazahstan (Voloshin et al. 1989). The arsenites were also found in the Urucum and Almerindo pegmatite mines and the Boca Rica claim, Minas Gerais, Brazil (Cassedanne 1986; https://www.mindat.org/), and in the White Elephant Mine, South Dakota, U.S.A. (Smith and Fritzsch 2000). In almost all these occurrences, they are associated with löllingite ± arsenopyrite ± tennantite. Lepageite and schafarzikite, from the Szklary pegmatite in Poland, are the third and fourth Fe-Mn arsenite-antimonite species known from a pegmatitic environment. Moreover, in the Szklary pegmatite, they coexist with three or four other Mn-Fe arsenite-antimonite species of different (Mn+Fe)/(As+Sb) ratio, still as yet undescribed due

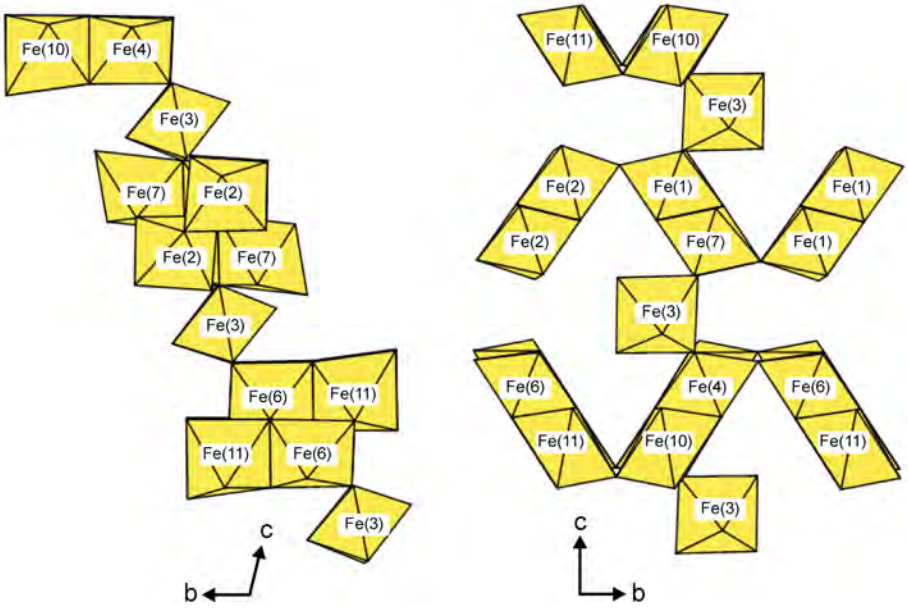

FIGURE 4. Components of the structure of lepageite: the extended linkage of $Fe^{2+}O_6$ octahedra. Legend as in Figure 2.

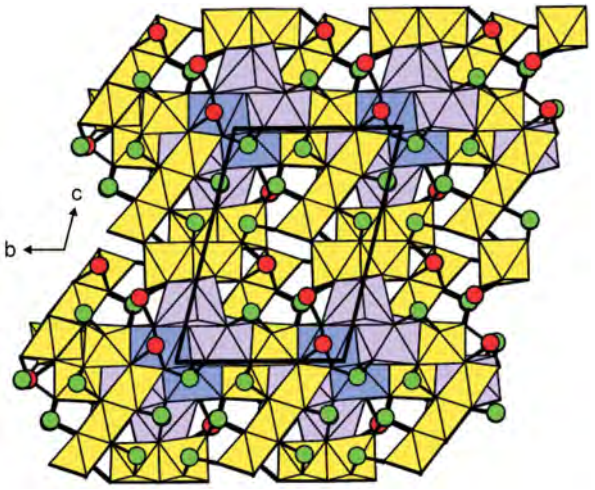

FIGURE 5. The crystal structure of lepageite. Legend as in Figure 2 plus green circles = Sb^{3+}; red circles = As^{3+}.

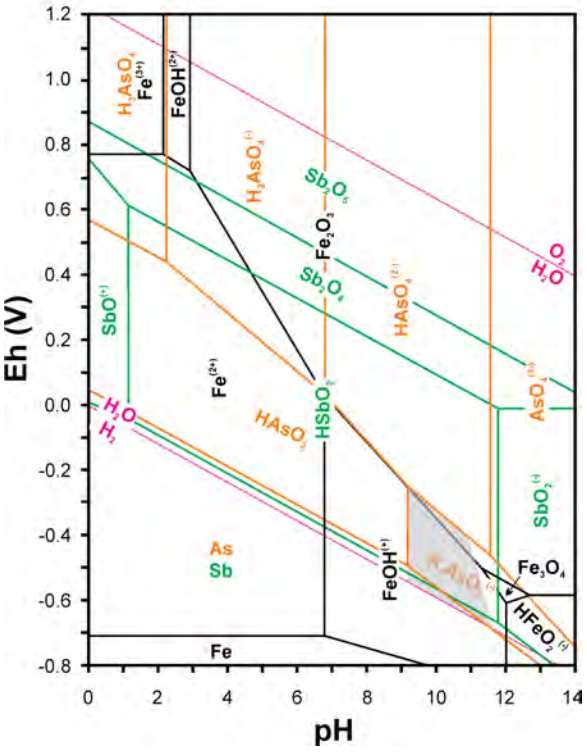

FIGURE 6. Crystallization conditions for arsenite-antimonite minerals in the Szklary pegmatite shown in the Eh–pH diagrams of Takeno (2005). The Eh–pH relations for Fe are marked in black, for As in orange, and for Sb in green. Manganese is omitted because it occurs as Mn^{2+} at pH < 10.5 and Eh < 0.2 V.

to their extremely small grain sizes. In this locality, lepageite and the other arsenite-antimonite phases crystallized from a geochemically evolved LCT-type melt related to anatectic melting in the nearby metasedimentary-metavolcanic GSB complex, emplaced into serpentinites of the Szklary massif as an adjacent part of the Sudetic ophiolite (Pieczka et al. 2015). The melt was strongly contaminated with Mg and enriched in fluid-mobile elements, particularly As and Sb, by interaction with the host serpentinite (see discussion on mobile elements in Deschamps et al. 2013; p.118). All these As and Sb minerals formed prior to the crystallization of beryl and cordierite-group minerals, and metasomatic alteration of the latter into an assemblage of (Mg,Cs)-enriched secondary beryl, mica-, chlorite-, and smectite-vermiculite-group minerals.

Characterization of the crystallization conditions for the arsenite-antimonite assemblage is an interesting problem as the Szklary pegmatite is unique with regard to the relatively numerous As ± Sb phases present. As arsenite-antimonite minerals are extremely rare in pegmatites, their appearance should be controlled by the As and Sb concentrations in pegmatite-forming melts, along with the coexisting S and accompanying redox conditions. Typical pegmatite-forming melts are usually poor in As and Sb, and these elements are generally completely incorporated by löllingite and arsenopyrite that form at high temperature early in the consolidation of a pegmatite. Geochemical fractionation can increase the concentrations of As and Sb to such a degree that, in the final stages of pegmatite formation at relatively high oxygen fugacity, they form Sb(As)-Nb-Ta oxides such as stibiocolumbite and stibiotantalite, or primary Sb-bearing pyrochlore-supergroup minerals, e.g., oxystibiomicrolite or members of the roméite group. The latter minerals involve partly or completely oxidized As and Sb. A good example of such behavior are the well-known pegmatites at Varuträsk (Sweden) with löllingite, arsenopyrite, stibnite, native Sb, stibarsen, senarmontite, stibiotantalite, and oxystibiomicrolite (Černý et al. 2004; Sandström 2008), at Viitaniemi (Finland) with löllingite, arsenopyrite, stibnite, tetrahedrite, native Sb, senarmontite, valentinite, and oxyplumboroméite (Sandström and Lahti 2009), at Urucum (Brazil) where karibibite and schneiderhöhnite are associated with löllingite, tennantite, and stibiotantalite (Cassedanne 1986), and at the White Elephant Mine, U.S.A., where schneiderhöhnite coexists with löllingite, arsenopyrite, and arsenolite (Smith and Fritzsch 2000).

The Szklary pegmatite has numerous droplet inclusions of native As and Sb, stibarsen and paradocrasite, As_2O_3 and Sb_2O_3 oxides, stibiocolumbite, and stibiotantalite as Sb^{3+}-(Nb,Ta) oxides, abundant substitution of As^{3+} and Sb^{3+} for Si^{4+} in dumortierite-supergroup minerals (Pieczka 2010; Pieczka et al. 2011, 2013), and the presence of schafarzikite, lepageite, and other unrecognized arsenite-antimonites. Furthermore, the presence of As^{5+} ± Sb^{5+} in (As,Sb)-bearing pyrochlores and apatites, chernovite-(Y) and arsenogorceixite, is unique. Moreover, the absence of sulfides and arsenides and the presence of exceptionally rare baryte only in the arsenite-antimonite assemblage are other important characteristics of the pegmatite.

The unique minerals of the Szklary pegmatite allow evaluation of the redox conditions of crystallization using Eh–pH diagrams for such redox-sensitive elements as As, Sb, and Fe, approximated to room temperature and $P = 10^5$ Pa (Takeno 2005). Superimposing these diagrams (Fig. 6) indicates that crystallization of As^{3+} and Sb^{3+} phases containing both Fe^{2+} and Fe^{3+} (as well as Mn^{2+}) occur at alkaline conditions (pH ≈ 9–11) at the relatively low reduction potential (Eh ≈ –0.7 to –0.3 V). This range of pH conditions corresponds to spring waters discharged from rocks undergoing active serpentinization, which typically have pH values even above 10 (McCollom and Seewald 2013). Above Eh > –0.4 to

–0.3 V, the $HAsO_4^{2-}$ species exists and arsenates should already crystallize in this pH range; at pH < 8, the $FeOH^+/Fe_2O_3$ and $HAsO_2/HAsO_4^{2-}$ equilibria superimpose, and thus $FeOH^+$ can only exist along with $HAsO_2$ with no ferric iron and arsenate species, or the species should occur together at slightly higher Eh. None of the latter situations corresponds to the assemblage recorded at Szklary, where tiny crystals of hematite are rarely associated with lepageite and the unrecognized arsenite-antimonite species as minute inclusions in (Mn,Be,Na,Cs)-bearing cordierite. The arsenite-antimonite assemblage also cannot crystallize at pH > 11, because magnetite should crystallize at these conditions (Fig. 6), and it is not observed at Szklary.

The conditions characterized above correspond to As and Sb transported in the alkaline fluids as $H_2AsO_3^-$ and $HSbO_2$ species and explain the initial formation of native As and Sb and their melts at the contacts with a more acidic felsic pegmatite-forming melt via the following redox reactions:

$$H_2AsO_3^- + 4H^+ + 3e^- = As + 3H_2O$$
$$HSbO_2 + 3H^+ + 3e^- = Sb + 2H_2O.$$

The change in pH caused by the alkaline fluids in the contact zone gave rise to successive crystallization of arsenite-antimonite phases, and finally to the appearance of As^{5+}- and Sb^{5+}-bearing species at increasing Eh, observed in the pegmatite only as products of the final crystallization: AsO_4-bearing apatite-group minerals, arsenogorceixite, chernovite-(Y), (As,Sb)-bearing pyrochlores, and coexisting baryte as a product of trace precipitation of $BaSO_4$ from oxidizing fluids carrying accessory sulfate anion. According to this scenario, arsenite-antimonite minerals can occur in granitic pegmatites only as accessory minerals, and this is what is observed.

Acknowledgments and Funding

We thank Anthony R. Kampf and an anonymous reviewer for valuable comments on this manuscript. The studies were supported by the National Science Centre (Poland) grant 2015/17/B/ST10/03231 and AGH-UST grant 16.16.140.315 to A.P. and a Discovery Grant to F.C.H. from the Natural Sciences and Engineering Research Council and a Grant from the Canada Foundation for Innovation to F.C.H.

References cited

Cassedanne, J.P. (1986) The Urucum pegmatite, Minas Gerais, Brazil. Mineralogical Record, 17, 307–314.

Černý, P., and Ercit, T.S. (2005) The classification of granitic pegmatites revisited. Canadian Mineralogist, 43, 2005–2026.

Černý, P., Chapman, R., Ferreira, K., and Smeds, S.A. (2004) Geochemistry of oxide minerals of Nb, Ta, Sn, and Sb in the Varuträsk granitic pegmatite, Sweden: The case of an "anomalous" columbite-tantalite trend. American Mineralogist, 89, 505–518.

Coda, A., Dal Negro, A., Sabelli, C., and Tazzoli, V. (1977) The crystal structure of stenhuggarite. Acta Crystallographica, B33, 1807–1811.

Cooper, M.A., and Hawthorne, F.C. (1996) The crystal structure of ludlockite, $PbFe_4^{3+}As_{10}^{3+}O_{22}$, the mineral with pentameric arsenite groups and orange hair. Canadian Mineralogist, 34, 79–89.

——— (2016) Refinement of the crystal structure of schneiderhöhnite. Canadian Mineralogist, 54, 707–713.

Deschamps, F., Godard, M., Guillot, S., and Hattori, K. (2013) Geochemistry of subduction zone serpentinites: A review. Lithos, 178, 96–127.

Gagné, O.C., and Hawthorne, F.C. (2015) Comprehensive derivation of bond-valence parameters for ion pairs involving oxygen. Acta Crystallographica, B71, 562–578.

——— (2018) Bond-length distributions for ions bonded to oxygen: Metalloids and post-transition metals. Acta Crystallographica, B74, 63–78.

Gaines, R.V., Skinner, H.C., Foord, E.E., Mason, B., and Rosenzweig, A. (1997) Dana's New Mineralogy, 8th ed. Wiley.

Larsen, A.O. (2013) Contributions to the mineralogy of the syenite pegmatites in the Larvik Plutonic Complex. Norsk Bergverksmuseet Skrift, 50, 101–109.

Le Page, Y. (1987) Computer derivation of the symmetry elements implied in a structure description. Journal of Applied Crystallography, 20, 264–269.

——— (1988) MISSYM 1.1—a flexible new release. Journal of Applied Crystallography, 21, 983–984.

Majerowicz, A., and Pin, C. (1986) Preliminary trace element evidence for an oceanic depleted mantle origin of the Ślęża ophiolitic complex SW Poland. Mineralogia Polonica, 17, 12–22.

Mandarino, J.A. (1979) The Gladstone-Dale relationship. Part III. Some general applications. Canadian Mineralogist, 17, 71–76.

——— (1981) The Gladstone-Dale relationship. Part IV. The compatibility concept and its application. Canadian Mineralogist, 19, 441–450.

McCollom, T.M., and Seewald, J.S. (2013) Serpentinites, hydrogen, and life. Elements, 9, 129–134.

Oliver, G.J.H., Corfu, F., and Krogh, T.E. (1993) U–Pb ages from SW Poland: evidence for a Caledonian suture zone between Baltica and Gondwana. Journal of Geological Society, London, 150, 355–369.

Pieczka, A. (2000) A rare mineral-bearing pegmatite from the Szklary serpentinite massif, the Fore-Sudetic Block, SW Poland. Geologia Sudetica, 33, 23–31.

——— (2010) Primary Nb-Ta minerals in the Szklary pegmatite, Poland: New insights into controls of crystal chemistry and crystallization sequences. American Mineralogist, 95, 1478–1492.

Pieczka, A., Grew, E.S., Groat, L.A., and Evans, R.J. (2011) Holtite and dumortierite from the Szklary pegmatite, Lower Silesia, Poland. Mineralogical Magazine, 75, 303–315.

Pieczka, A., Evans, R.J., Grew, E.S., Groat, L.A., Ma, C., and Rossman, G.R. (2013) The dumortierite supergroup. II. Three new minerals from the Szklary pegmatite, SW Poland: Nioboholtite, $(Nb_{0.6}\square_{0.4})Al_6BSi_3O_{18}$, titanoholtite, $(Ti_{0.75}\square_{0.25})Al_6BSi_3O_{18}$, and szklaryite, $\square Al_6BAs_3^{3+}O_{15}$. Mineralogical Magazine, 77, 2841–2856.

Pieczka, A., Szuszkiewicz, A., Szełęg, E., Janeczek, J., and Nejbert, K. (2015) Granitic pegmatites of the Polish part of the Sudetes (NE Bohemian massif, SW Poland). Fieldtrip Guidebook of the 7th International Symposium on Granitic Pegmatites, Książ, Poland, June 17-19 (2015) C 73–103.

Pieczka, A., Biagioni, C., Gołębiowska, B., Jeleń, P., Pasero, M., and Sitarz, M. (2018) Parafiniukite, $Ca_2Mn_3(PO_4)_3Cl$, a new member of the apatite supergroup from the Szklary pegmatite, Lower Silesia, Poland: Description and crystal structure. Minerals, 9, 485.

Pouchou, I.L., and Pichoir, F. (1985) "PAP" (phi-rho-z) procedure for improved quantitative microanalysis. In I.T. Armstrong, Ed., Microbeam Analysis, p. 104–106. San Francisco Press.

Sandström, F. (2008) Varuträskpegmatiten. Litofilen, 25(2), 17–46 (in Swedish).

Sandström, F., and Lahti, S.I. (2009) Viitaniemipegmatiten i Eräjärvi, Orivesi, Finland. Litofilen, 26(1), 11–38.

Smith, A.E., and Fritzsch, E. (2000) South Dakota. Rock & Minerals, 75(3), 156–169.

Strunz, H., and Nickel, E.H. (2001) Strunz Mineralogical Tables, 9th ed. Schweizerbart'sche Verlagsbuchhandlung, Stuttgart.

Szuszkiewicz, A., Pieczka, A., Gołębiowska, B., Dumańska-Słowik, M., Marszałek, M., and Szełęg, E. (2018) Chemical composition of Mn- and Cl-rich apatites from the Szklary pegmatite, Central Sudetes, SW Poland: Taxonomic and genetic implications. Minerals, 8, 350.

Takeno, N. (2005) Atlas of Eh-pH diagrams. Intercomparison of thermodynamic databases. Geological Survey of Japan Open File Report No.419. National Institute of Advanced Industrial Science and Technology; Research Center for Deep Geological Environments.

Timmermann, H., Parrish, R.R., Noble, S.R., and Kryza, R. (2000) New U–Pb monazite and zircon data from the Sudetes Mountains in SW Poland: evidence for a single-cycle Variscan orogeny. Journal of the Geological Society, London, 157, 265–268.

Turniak, K., Pieczka, A., Kennedy, A.K., Szełęg, E., Ilnicki, S., Nejbert, K., and Szuszkiewicz, A. (2015) Crystallisation age of the Julianna pegmatite system (Góry Sowie Block, NE margin of the Bohemian massif): evidence from U-Th-Pb SHRIMP monazite and CHIME uraninite studies. Book of Abstracts of the 7th International Symposium on Granitic Pegmatites, Książ, Poland, 111–112.

Van Breemen, O., Bowes, D.R., Aftalion, M., and Żelaźniewicz, A. (1988) Devonian tectonothermal activity in the Sowie Góry gneissic block, Sudetes, southwestern Poland: evidence from Rb-Sr and U-Pb isotopic studies. Journal of Polish Geological Society, 58, 3–10.

Voloshin, A.V., Pakhomovsky, Ya.A., and Bakhchisaraitsev, A.Yu. (1989) On karibibite and schneiderhohnite from pegmatites of Eastern Kazakhstan. Novye Dannye o Mineralakh, Moscow, Nauka, 36, 129–135 (in Russian).

Manuscript received November 20, 2018
Manuscript accepted March 28, 2019
Manuscript handled by Fabrizio Nestola

Endnote:

[1]Deposit item AM-19-76903, Supplemental Material and CIF. Deposit items are free to all readers and found on the MSA website, via the specific issue's Table of Contents (go to http://www.minsocam.org/MSA/AmMin/TOC/2019/Jul2019_data/Jul2019_data.html).